Title
Complete characterization of a lithium battery electrolyte using a combination of electrophoretic NMR and electrochemical methods

Journal
Physical Chemistry Chemical Physics, 24(43)

ISSN
1463-9076

Authors
Hickson, Darby T
Halat, David M
Ho, Alec S
et al.

Publication Date
2022-11-09

DOI
10.1039/d2cp02622h

Peer reviewed

Complete Characterization of a Lithium Battery Electrolyte using a Combination of Electrophoretic NMR and Electrochemical Methods

Darby T. Hickson,[1,2] David M. Halat,[1,2] Alec S. Ho,[1,2] Jeffrey A. Reimer,[1,2] Nitash P. Balsara[1,2]
[1]*Materials Sciences Division, Lawrence Berkeley National Laboratory, Berkeley, California 94720, United States*
[2]*Department of Chemical and Biomolecular Engineering, University of California, Berkeley, Berkeley, California 94720, United States*

ABSTRACT

Improving transport properties of the electrolyte is important for developing lithium-ion batteries for future energy storage applications. In Newman's concentrated solution theory, electrolytes are characterized by three transport parameters, conductivity, diffusion coefficient, and transference number, in addition to the thermodynamic factor. In this work, these parameters are all determined for an exemplar liquid electrolyte, lithium bis(trifluoromethanesulfonyl)imide mixed in tetraethylene glycol dimethyl ether, using electrochemical methods. The intrinsic coupling between parameters obtained by electrochemical methods results in large error bars in the transference number that obscure the transport behavior of the electrolyte. Here, we use electrophoretic NMR (eNMR) to measure the electric-field-induced ion and solvent velocities to obtain the transference number directly, which enables determination of the thermodynamic factor with greater certainty. Our work indicates that the combination of eNMR and electrochemical methods provides a robust approach for complete characterization of battery electrolytes.

INTRODUCTION

Over the last decade, the sale and use of electric vehicles (EVs) has dramatically increased due to the improvement in lithium-ion batteries. Batteries for electric vehicles still need to bolster reliability and range in order to appeal to the consumer, which requires improvement in battery technology related to safety, cost, discharge rates, and energy density.[1] The state-of-the-art lithium-ion battery includes a graphitic anode, a carbonate-based liquid electrolyte, and a transition-metal-oxide cathode. Modeling ion transport through the battery requires complete characterization of the electrolyte, which comprises a lithium salt dissolved in an organic solvent (or a mixture of organic solvents). In Newman's concentrated solution theory,[2] complete characterization implies knowledge of the thermodynamic factor and three transport parameters – conductivity, κ, salt diffusion coefficient, D, and the cation transference number with respect to the solvent velocity, t_{+}^{0}. Conductivity and salt diffusion coefficient are relatively easy to measure: κ is measured by ac impedance spectroscopy and D is measured by restricted diffusion. Data from each of these experiments can be used to determine κ and D directly. In contrast, the transference number is difficult to measure accurately because it typically requires combining three or four separate electrochemical experiments, depending on the particular approach used.[3-7] Similar difficulties apply to the thermodynamic factor.

The thermodynamic factor, T_f, is defined as[2]

$$T_f = 1 + d\ln\frac{\gamma_{\pm ¿}}{d\ln m}, ¿ \quad (1)$$

where $\gamma_{\pm ¿¿}$ is the mean molal activity coefficient of the salt and m is the molality of the electrolyte. An experiment that is often used to determine the thermodynamic factor involves a concentration cell,[8] shown schematically in Figure 1. The cell comprises two compartments separated by a porous glass frit. Two solutions at different molalities, m andm_r, are placed in the two compartments, and the open circuit potential, U, is measured using lithium metal electrodes. Care is taken to ensure that the measurements are made before significant diffusion occurs across the glass frit. For a univalent salt, the relationship between U and $\gamma_{\pm ¿¿}$ is given by equation 2,[2]

$$FU = 2RT\int_{m_r}^{m} t_{-¿^0¿¿}¿ \quad (2)$$

Equation 2 may be used to determine the dependence of $\gamma_{\pm ¿¿}$ on m, but this requires knowledge of the anion transference number, $t_{-¿^0¿}$, at all concentrations between m_r and m. This knowledge is traditionally obtained by additional electrochemical experiments as demonstrated first by Ma et al.[3] In ref. 3, the additional experiment used was the current interrupt technique wherein a constant current density, i, is applied to a lithium-electrolyte-lithium symmetric cell for a short period of time, t, and the open circuit potential right after the current is interrupted, U_{ci}, is measured as a function of applied current density. The slope of a plot of U_{ci} versus $it^{1/2}$ is related to $t_{+¿^0¿}$. However, in addition to the transference number, this slope also depends on D and T_f. One therefore needs a third experiment to measure D. In the work of Ma et al., the restricted diffusion experiment was used to determine D. In related work, Pesko et al. used measurements of the current fraction, $\rho_{+¿¿}$, as the additional experiment for determining $t_{+¿^0¿}$.[4] $\rho_{+¿¿}$is defined as the ratio of the steady state current to the initial current measured in a lithium-electrolyte-lithium symmetric cell. The importance of $\rho_{+¿¿}$ was recognized in the pioneering works of Bruce and coworkers[9,10] and Watanabe and coworkers.[11] The uncertainty in the measured transference number using either electrochemical method discussed in this paragraph is large because of its dependence on multiple parameters with their own experimental error.[12]

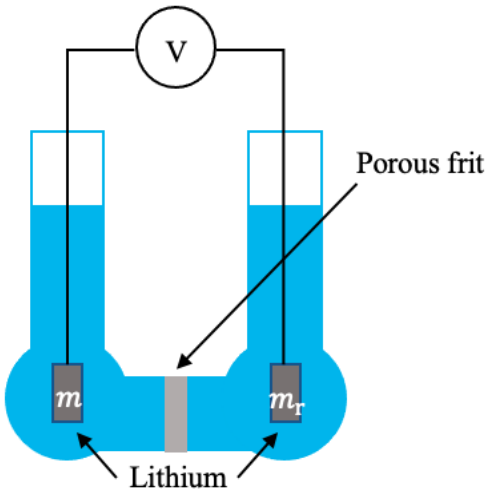

Figure 1. Schematic of a concentration cell.

One additional problem arises when lithium-electrolyte-lithium symmetric cells are used to obtain transport properties. Most liquid electrolytes react irreversibly with lithium metal, especially under applied electric fields, and this results in the formation of a variety of protrusions, such as dendrites, globules, and mossy and tree-like structures.[13,14] While the importance of these structures in the context of commercializing rechargeable batteries with lithium metal electrodes has received considerable attention, their relevance in the context of electrolyte characterization is seldom discussed. The expressions used to analyze the data from symmetric cells to obtain t_{+}^{0}, D, U_{ci}, and ρ_{+} are invalid if the lithium electrodes are nonplanar.

The objective of this paper is to present a new approach for complete characterization of liquid electrolytes. The electrolyte chosen for this study is a mixture of lithium bis(trifluoromethanesulfonyl)imide (LiTFSI) salt in tetraethylene glycol dimethyl ether (tetraglyme). Our work adds to the body of knowledge that already exists on ion transport in LiTFSI/tetraglyme mixtures.[15-18] The application of electrophoretic NMR (eNMR) to electrolytes is well established.[19-21] eNMR directly measures the velocities of the cation, v_{+}, anion, v_{-}, and the solvent, v_0, under an applied electric field. It has been shown[22] using concentrated solution theory that

$$t_{+}^{0} = \frac{v_{+} - v_0}{v_{+} - v_{-}} \tag{3}$$

The measured species' velocities in equation 3 are ensemble averages over all the different environments present in the electrolyte. This includes disassociated individual ions, charged clusters containing ions, charged solvent-ion clusters, and uncharged clusters like ion pairs. Since the average species' velocities can be measured with high precision, t_{+}^{0} values obtained by this technique have small uncertainties. This in turn enables determination of the thermodynamic factor using concentration cells as shown in equation 2; the uncertainty in T_f thus obtained is also smaller than that obtained by combining three electrochemical experiments. We also present measurements of κ using blocking electrodes, D using restricted diffusion, and

$\rho_{+/-}$ using symmetric cells. This enables comparison of measured values of T_f and $t_{+/-}^0$ determined by the eNMR/electrochemical combination and those determined solely by electrochemical methods.–Although eNMR has previously been used to characterize many different liquid electrolytes,[17,21] it has not yet been combined with electrochemical methods to completely characterize ion transport.

In addition to performing electrochemical and eNMR experiments, we have quantified the nature of the lithium-tetraglyme interfaces in cycled symmetric cells using hard X-ray microtomography. X-ray tomography is a 3D, nondestructive imaging technique[23] that has been used to image a variety of electrochemical cells to study phenomena such as electrode expansion[24] and dendrite growth in cells containing both liquid[25,26] and polymer electrolytes.[27] The results of these experiments ensure the validity of expressions used to obtain transport parameters from data obtained in lithium-LiTFSI/tetraglyme-lithium symmetric cells.

EXPERIMENTAL

Electrolyte Preparation

Tetraethylene glycol dimethyl ether (tetraglyme) and lithium bis(trifluoromethanesulfonyl)imide (LiTFSI) salt were obtained from Sigma-Aldrich and dried under active vacuum in a glovebox antechamber for three days at 60˚C and 100˚C, respectively. All electrolytes were made in an argon glovebox, with water and oxygen levels kept below 1 ppm. Electrolytes were prepared by dissolving a known mass of LiTFSI salt in a given volume of tetraglyme and stirring overnight at 25˚C. Concentrations of electrolyte varied between an r value of 0.008 and 0.112, where r is a measure of salt concentration corresponding to the ratio of lithium ions to ether oxygens in tetraglyme, r = ([Li^+]/[O]). We also provide salt concentration in units of molality (moles of LiTFSI per kilogram of tetraglyme), m. The concentrations used in this study are summarized in Table S1.

Conductivity

Conductivity was measured using a Mettler Toledo InLab-751 conductivity probe with platinum blocking electrodes. Temperature was measured via the probe and maintained at 30˚C ± 1˚C during the measurement. The conductivity probe was calibrated using a 1413 μS/cm potassium chloride conductivity standard to determine the cell constant prior to measurement. Conductivity was also measured using ac impedance spectroscopy. Five layers of Celgard 2500 separators soaked in electrolyte were sandwiched between stainless steel shims (MTI Corp.) and assembled in CR2032 coin cell parts (MTI Corp). The Celgard separators were cut to 19 mm and have a thickness of 25 μm. The stainless steel shims had a diameter of 15.5 mm and a thickness of 0.2 mm. Cells were made in triplicate for each concentration and cycled in an environmental chamber to maintain a temperature of 30˚C. Impedance measurements were taken using a Biologic VMP300 potentiostat, where impedance spectra were obtained for a frequency range of 100 mHz to 1 MHz with a voltage amplitude of 5 mV. Series resistance values, R_s, were obtained from the impedance spectra and related to the conductivity via:

$$\kappa = \frac{\tau}{\varphi_c}\frac{l}{R_s A}, \tag{4}$$

where τ is the separator tortuosity, φ_c is the volume fraction of the conducting phase, l is the thickness of the separator, and A is the surface area of the electrodes. For Celgard 2500, φ_c is taken as 0.55, the porosity according to the manufacturer. The utilization of two conductivity measurements enables the determination of τ for the Celgard separator:[28] τ = 2.93.

Current Fraction and Restricted Diffusion

Polarization experiments were performed on lithium-LiTFSI/tetraglyme-lithium symmetric cells assembled in coin cells. Layers of five or ten Celgard 2500 separators were soaked in electrolyte and stacked between 14 mm lithium chips with a thickness of 600 μm (MTI Corp). The cell stack was topped with a 15.5 mm stainless steel shim and a wave spring before crimping. At least three cells were made for each thickness and concentration. Cells were cycled inside an environmental chamber to maintain a temperature of 30˚C, which was corroborated using a thermocouple.

To establish a stable solid electrolyte interphase (SEI) between lithium metal and the electrolyte, cells were preconditioned by positively polarizing the cell at 0.02 mA/cm^2 for four hours, letting the cell rest for one hour, and negatively polarizing the cell at 0.02 mA/cm^2 for four hours. Six conditioning cycles were performed to stabilize the interfacial resistance. After conditioning, the cell was polarized at ΔV = 10 mV, -10 mV, 20 mV, and -20 mV to make sure measurements were independent of applied potential. To obtain the current fraction, the steady-state current, I_{ss}, was measured for one hour and impedance measurements were taken every 20 minutes, including before and after polarization. The current fraction was then determined using equation 5.[9,10,29]

$$\rho_{+,¿} = \frac{I_{ss}}{I_\Omega}\left(\frac{\Delta V - I_\Omega R_{i,0}}{\Delta V - I_{ss} R_{i,ss}}\right)_{,¿} \tag{5}$$

$R_{i,0}$ and $R_{i,ss}$ are the interfacial resistance before polarization and after I_{ss}, the steady state current, has been reached. I_Ω is the initial current in the cell, calculated by dividing the applied polarization, ΔV, by the summation of the initial bulk and interfacial resistances in the cell. This calculation is based on Ohm's law, assuming no concentration gradients exist at the first instant of polarization in the cell.

The diffusion coefficient was measured using restricted diffusion.[30] After polarization, the cell was allowed to relax for one hour and the open circuit potential (OCV) was measured every 0.5 seconds. The relaxation of the concentration gradient in the cell was measured via the relaxation of the potential. This was fitted to an exponential, $U(t) = k_0 + a e^{-bt}$, where k_0 is an offset voltage and a and b are fit parameters; $1/b$ is the characteristic decay time. The diffusion coefficient through the separator, D_s, was determined using the following equation, $D_s = \frac{l^2 b}{\pi^2}$. The relaxation potential is fit over a time window such that $\alpha = \frac{D_s t}{l^2} > 0.03$, which ensures the fit is independent of the shape of the steady-state concentration gradient formed during polarization.[31] For the five Celgard cells, D_s was obtained from the first 15 minutes of the relaxation profile. For the ten Celgard cells, D_s was obtained from the first 60 minutes of the

relaxation profile. This is because increasing l by a factor of two results in a fourfold increase in characteristic decay time. The salt diffusion coefficient was calculated by correcting D_s for the tortuosity of the separator, so that $D = \tau D_s$.

Concentration Cells

The thermodynamic factor was determined using concentration cells[8] as described previously. Custom made glass U-cells were obtained from Adams and Chittenden. The U-cells contain a porous glass frit separating the two chambers to prevent rapid mixing, with an average pore size of 1.0-1.6 μm. One side of the U-cell was filled with a reference electrolyte (r = 0.064) and the other side filled with a test concentration. Each side was filled with equal volumes of electrolyte to equilibrate the heights in the two chambers and minimize pressure differences. Lithium electrodes were submerged into each side of the U-cell and the OCV was measured for one hour for each test concentration to ensure the potential plateaued. Electrodes were connected so that a positive potential was measured when $m_r > m$. Measurements were taken at least twice for each concentration. Temperature was maintained at 30°C ± 1°C for the duration of the experiment.

Cell Design for X-ray tomography

Lithium-LiTFSI/tetraglyme-lithium symmetric cells were assembled in an airtight custom made cell holder made from polyether ethyl ketone (PEEK) as described by Ho et al.[32] The cell consisted of a 4 mm diameter lithium electrode, one 5 mm diameter Celgard 2500 separator soaked in electrolyte (r = 0.032), and another 4 mm diameter lithium electrode. Lithium electrodes had a thickness of 300 μm. A stainless steel spacer was placed on top of the stack to protect the lithium from deformation. The entire stack was topped with a spring and placed between stainless steel current collecting pins. Various cycling treatments were used to study the effect of current density, i, on lithium plating. One cell was uncycled to image the clean interface. Another cell underwent preconditioning only, five cycles of $i = \pm 0.01$ mA/cm^2 for four hours each. Tomographic imaging was conducted in accordance with the work done by Maslyn et al[33] at Beamline 8.3.2 at the Advanced Light Source at Lawrence Berkeley National Laboratory.

Electrophoretic NMR

eNMR experiments were conducted in accordance with the method described by Halat et al.[34] The design and execution of eNMR experiments is discussed elsewhere.[19,35] ^{7}Li, ^{19}F, and ^{1}H NMR measurements were used to determine cation, anion, and solvent velocities, respectively. All experiments were conducted at 30°C.

RESULTS AND DISCUSSION

X-ray tomography was used to study the electrode-electrolyte interfaces in lithium-LiTFSI/tetraglyme-lithium symmetric cells. A Celgard separator was used to construct the cells (see experimental section). In Figure 2a, we show a typical cross-sectional slice through an uncycled cell. Here we see two clean planar interfaces between the electrode and the electrolyte. In Figure 2b, we a show a typical tomographic slice through a preconditioned symmetric cell cycled at i = 0.01 mA/cm^2. This represents the typical polarization experiment for electrochemical characterization. The two clean interfaces seen in Figure 2b indicate that

expressions for interpreting electrochemical data from symmetric cells with planar electrodes are valid. We note in passing that mossy lithium deposits can be seen in tomographic cross-sectional images obtained from cells cycled at $i = 0.1$ mA/cm^2; these images are not shown for brevity.

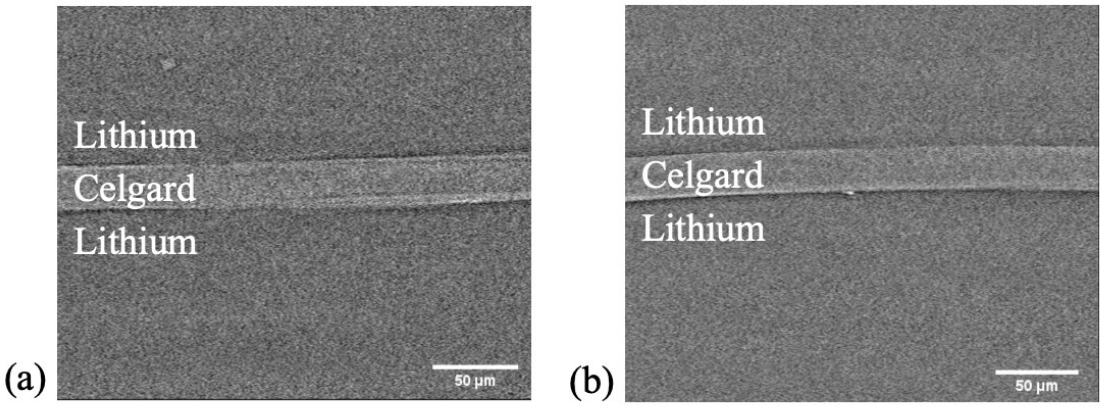

Figure 2. Typical tomographic slices of a lithium-LiTFSI/tetraglyme soaked Celgard separator-lithium symmetric cell. Comparison of an uncycled cell (2a) and a preconditioned cell (2b). No discernible mossy lithium is present when the cell undergoes low current cycling for short cycling times.

In Figure 3a, we plot conductivity, κ, as a function of both salt concentration, r, and molality, m, shown in the top x-axis. The figure shows conductivity values obtained using the conductivity probe and coin cells with blocking electrodes. Good agreement between the two methods is seen across the concentration range. Conductivity shows a nonmonotonic dependence on concentration, with an increase at low concentrations until a maximum is reached, and then a decrease across the rest of the concentration range. Conductivity increases at low concentrations due to the increase in the number of charge carriers. At higher salt concentrations, the increase in viscosity causes a decrease in the overall conductivity. In Figure 3b, we plot the current fraction, $\rho_{+¿¿}$, as a function of r and m. $\rho_{+¿¿}$generally decreases with increasing r. The values of $\rho_{+¿¿}$ are small, usually below 0.20. The reproducibility of the measurement at $r = 0.01$ is low, presumably due to the low concentration of charge carriers. In Figure 3c, we plot the diffusion coefficient, D, as a function of r and m. Within experimental error, D is independent of r, taking on values between 2×10^{-7} to 7×10^{-7} cm^2/s. We have averaged data obtained from both five and ten Celgard cells; data from both kinds of cells were more-or-less consistent with each other; individual data sets obtained from the two types of Celgard cells are shown in Figure S2.1. The data in Figures 3c and S2.1 differ substantially from the measurements of Fawdon et al., who determined D from time resolved Raman microscopy.[36] Such discrepancies are often found in the literature.[6, 37, 38] Further work is needed to resolve such discrepancies. In Figure 3d, we plot U as a function of $\ln m$. The variance of measured values of U is significantly smaller than that of the other parameters in Figure 3. U is a monotonic function of $\ln m$. The general characteristics of the U versus $\ln m$ data in Figure 3d are similar to those published previously on mixtures of LiTFSI in poly(ethylene oxide).[4] This is not surprising because of the similarity in the chemical structures of tetraglyme and poly(ethylene oxide).

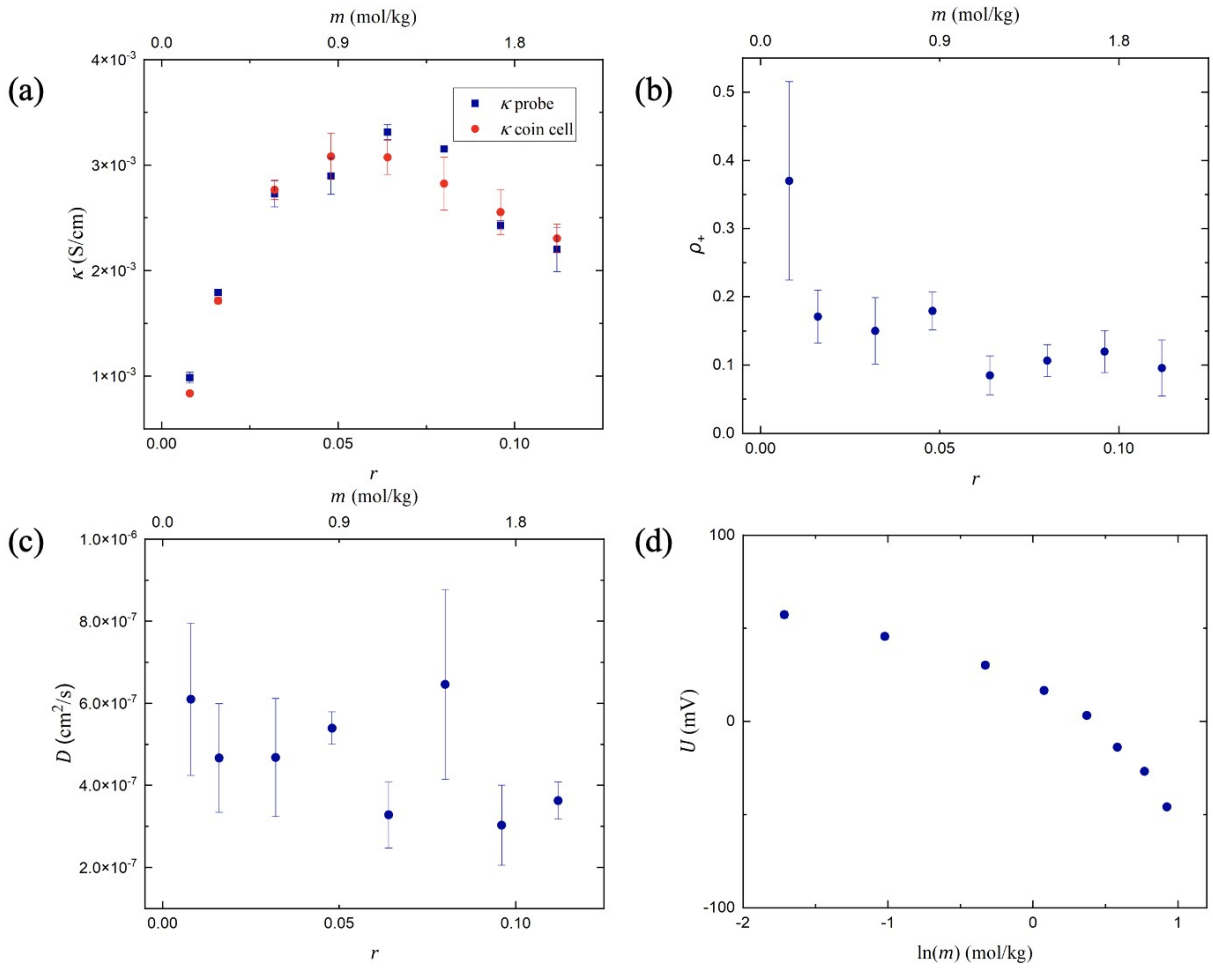

Figure 3. Electrochemical data for LiTFSI/tetraglyme, including a) conductivity as a function of r obtained using a conductivity probe and ac impedance spectroscopy; b) current fraction as a function of r obtained using polarization experiments; c) salt diffusion coefficient as a function of r determined from restricted diffusion; d) open circuit potential as a function of log of molality obtained using concentration cells with a reference concentration of r = 0.064. All data was collected at 30˚C.

For a univalent salt, the differential form of equation 2 is used to relate U, T_f, and $t_{+¿^0¿}$.[2]

$$T_f = \frac{-F}{2RT¿¿} \tag{6}$$

The term ¿can be expressed in terms of measured parameters κ, D, $\rho_{+¿¿}$, and U to give:[39,40]

$$T_f = \frac{\kappa}{2RTDc¿¿} \tag{7}$$

To calculate $\frac{dU}{d\ln m}$ at a given m, we use a finite difference approach. At all of the concentrations except the lowest and highest concentrations, $\frac{dU}{d\ln m}$ is taken to be the average of the finite difference slopes obtained on either side of that concentration. At the lowest and highest concentration, $\frac{dU}{d\ln m}$ is based on a single slope. This enables determination of T_f as a function

of
m. Finally, $t_{+¿^0¿}$ can be determined as a function of m using equation 8,[39,40]

$$t_{+¿^0=1-\sqrt{\frac{F^2 Dc}{2\kappa RT T_f}}¿¿¿} \quad (8)$$

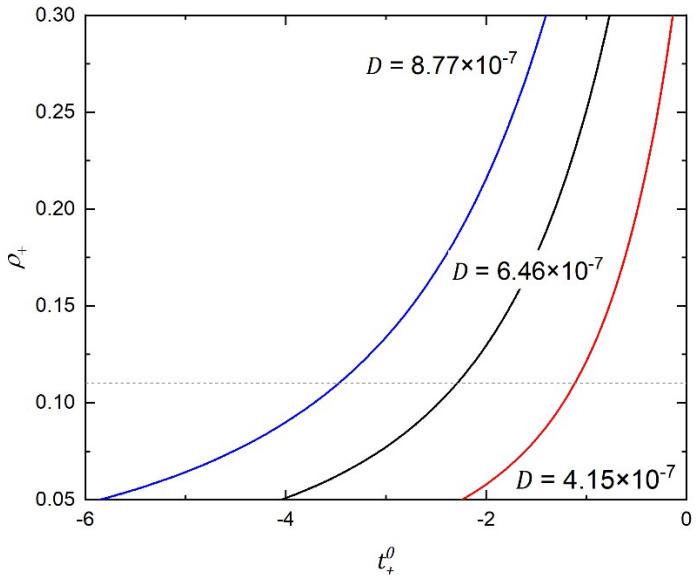

Figure 4. Dependence of the current fraction on the transference number for fixed transport parameters (r = 0.08, c = 0.00152 mol/cm^3, κ = 3.15×10^{-3} S/cm). Calculations are shown for three values of D, as indicated on the figure, and corresponding values of T_f. The dashed line at $\rho_{+¿¿}$ = 0.11 corresponds to the average value of the current fraction at this salt concentration.

Accurate determination of the transference number using multiple electrochemical experiments is difficult due to the compounding of errors. The transference number depends on three measured parameters, $\rho_{+¿¿}$, D, and κ, and one indirectly measured parameter, T_f (see equation 8). It is evident from Figure 3 that the variability in the measured values of $\rho_{+¿¿}$ and D is larger than that of the measured values of κ and U. In Figure 4, we thus focus on how $t_{+¿^0¿}$ depends on $\rho_{+¿¿}$ and D.[41] For concreteness, we have used the measured parameters for r = 0.08 and the dependence of $\rho_{+¿¿}$ on $t_{+¿^0¿}$ for selected values of D is shown in Figure 4. These selected values cover the uncertainty in D reported in Figure 3c. At this value of r, the average value of $\rho_{+¿¿}$ is 0.11. However, individual experiments gave $\rho_{+¿¿}$ values as high as 0.15 and values as low as 0.07. It is evident from Figure 4 that the estimated value of $t_{+¿^0¿}$ is greatly influenced by the assumed value of D. A $t_{+¿^0¿}$ value of -1.1 is obtained using D = 4.15×10^{-7}. In contrast, a $t_{+¿^0¿}$ value of -3.5 is obtained using D = 8.77×10^{-7}. This uncertainty increases rapidly as $\rho_{+¿¿}$ decreases. It is important to note that uncertainties in $\rho_{+¿¿}$ and D are only two of the four sources of uncertainty in $t_{+¿^0¿}$. There is clearly a need to explore other avenues for determining $t_{+¿^0¿}$. It is widely accepted that values of $t_{+¿^0¿}$ in the vicinity of 0 or lower imply the presence of complex clusters involving multiple ions and solvent molecules.[42,43] Not only are these systems challenging to model, they are also difficult to study from the characterization point of view due to complex interactions between different species (cations, anions, and solvent) within the electrolyte.[2,3,11,15,17,34,43,44]

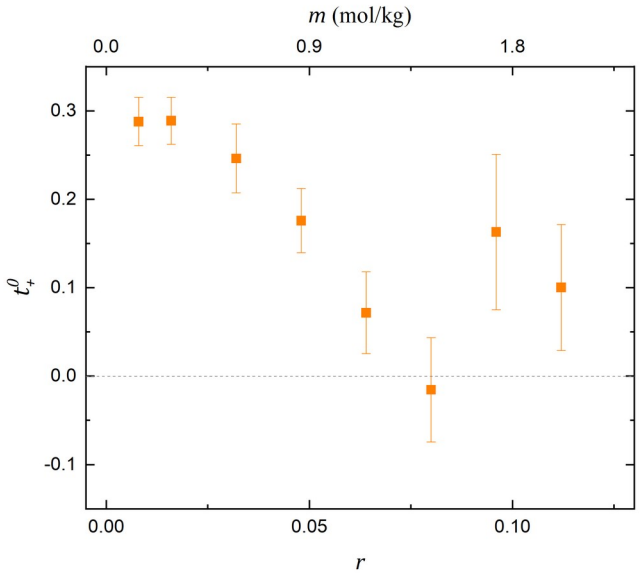

Figure 5. The transference number as a function of m and r determined from eNMR.

The transference number can also be measured directly using eNMR.[19-21] In this technique, velocities for the cation, anion, and solvent are directly measured and used to calculate the transference number according to equation 3. The dependence of $t_{+¿^0¿}$ on m determined by this method is shown in Figure 5. The transference number has a nonmonotonic dependence on concentration; it decreases at low concentrations until a minimum close to 0 is reached at $r = 0.08$ and then increases again. $t_{+¿^0¿}$ value of 0 implies that under an applied electric field, the solvent and cation velocity are the same, suggesting strong complexation between all lithium ions and solvent molecules.[34] The increase of $t_{+¿^0¿}$ above $r = 0.08$ indicates the presence of more complex solvation structures and ion clustering.

In Figure 6a, we compare transference numbers determined by eNMR based on equation 3, referred to as $t^0_{+,\,eNMR}$, and electrochemical methods based on equation 8, referred to as $t^0_{+,\,echem}$. The electrochemical data showed no evidence of a systematic dependence of $t_{+¿^0¿}$ on r. $t^0_{+,\,echem}$ reaches a minimum at $r = 0.08$. This is qualitatively similar to $t^0_{+,\,eNMR}$, which also shows a minimum at the same salt concentration. The absolute values of $t_{+¿^0¿}$ obtained by the two methods, however, are very different. Whereas $t_{+¿^0¿}$ from eNMR is positive over the salt concentration range, $t_{+¿^0¿}$ determined by electrochemical methods is almost exclusively negative. If our methods to estimate the uncertainty of $t_{+¿^0¿}$ by electrochemical methods were robust, we would expect the error bars corresponding to these values to include more accurately determined values of $t_{+¿^0¿}$ based on eNMR. We posit that our methods to estimate the uncertainty in our electrochemical characterization, which assumes that the errors in the four parameters needed to calculate $t_{+¿^0¿}$ are independent, are inadequate. Our results for $\rho_{+¿¿}$ and D are based on three replicates for each salt concentration and cell thickness, while our results for κ and $\frac{dU}{dlnm}$ are based on three and two replicates, respectively, measured in the same cell geometry. Perhaps increasing the number of samples by an order of magnitude would result in more robust estimates of error bars. It seems likely that our assumption regarding the independence of individual errors is too simplistic. Additional complications may arise in liquid electrolytes due

to the need for a separator, convection effects, and instability of the electrode-tetraglyme interface.

Accurate determination of $t_{+,0}$ also leads to accurate determination of T_f. In Figure 6b, we plot the thermodynamic factor determined using equation 6 with $t_{+,0}$ determined by eNMR. Also included in this figure is the thermodynamic factor determined using equation 7, which relies on four electrochemical characterization experiments. The former is referred to as $T_{f,eNMR}$ and the latter $T_{f,echem}$. While there are discrepancies between $T_{f,eNMR}$ and $T_{f,echem}$, they are significantly smaller than those between $t^0_{+,eNMR}$ and $t^0_{+,echem}$. Both thermodynamic factors are assumed to be equal to unity at $r = 0$, as required by thermodynamics. They both decrease up to $r \cong 0.025$ and then increase over the rest of the concentration range. Measurements of T_f indicate that the electrolyte is non-ideal. The decrease of T_f to values below unity at low concentrations reflects Debye-Huckel interactions[2,45], which dominate dilute electrolytes. The increase of T_f at higher concentrations reflects more complex ion-ion and ion-solvent interactions. Whereas measurement of $T_{f,echem}$ requires knowledge of four measured quantities (see equation 7), measurement of $T_{f,eNMR}$ only requires knowledge of two parameters determined from independent experiments: $t_{+,0}$ from eNMR and $\frac{dU}{d\ln m}$ from concentration cell experiments (see equation 6). Neither of these methods require stripping and plating of lithium metal, which eliminates any complications related to the reactive interface. While the dependence of $T_{f,echem}$ and $T_{f,eNMR}$ on salt concentration is similar, $T_{f,eNMR}$ is significantly larger that □, especially at high salt concnetrations.

The diffusion coefficient, D, gives the flux of salt based on concentration gradients. This transport parameter is affected by both frictional and thermodynamic effects. We expect D to decrease with increasing r due to the increase in frictional effects. However, the significant increase in the thermodynamic factor with increasing r (Figure 6b) indicates that the gradient in chemical potential corresponding to the same concentration gradient increases with increasing r; this increase is larger in when eNMR results are included in the analysis. ~~.~~ The~~se two~~ frictional the thermodynamic effects cancel out, resulting in a diffusion coefficient that is, at best, a weak function of r (Figure 3c).

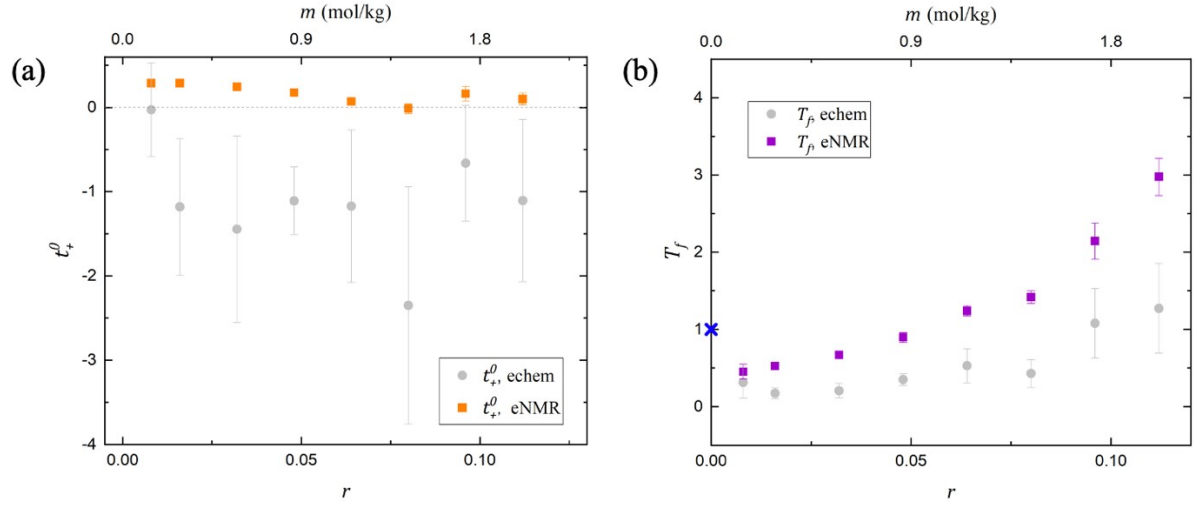

Figure 6. Comparison of electrochemical techniques and electrophoretic NMR for (a) transference number and (b) thermodynamic factor. The thermodynamic factor is unity at $r = 0$, shown in blue, based on the thermodynamic requirement that all solutions are ideal in the limit of infinite dilution.

CONCLUSIONS

In this work we present complete electrochemical characterization of the bulk transport properties for an exemplar liquid electrolyte, LiTFSI salt dissolved in tetraglyme. Experiments included measurement of κ using ac impedance spectroscopy, D using restricted diffusion, $\rho_{+¿¿}$ using polarization experiments, and $\frac{dU}{d\ln m}$ using concentration cells. The results of these four experiments were combined to give estimates of $t_{+¿^0¿}$ and T_f. We also measured $t_{+¿^0¿}$ directly from eNMR measurements of ion and solvent velocities. The eNMR experiment requires specialized instrumentation while electrochemical characterization can be performed on commercially available potentiostats. We then used these measurements to determine T_f from concentration cell data. By combining eNMR and electrochemical techniques, we present complete electrochemical characterization of a liquid electrolyte with much smaller uncertainty in both $t_{+¿^0¿}$ and T_f.

AUTHOR CONTRIBUTIONS

D. M. H performed and analyzed electrophoretic NMR experiments. A. S. H. performed x-ray tomography experiments. D. T. H. performed and analyzed electrochemical experiments. D. T. H. and N. P. B interpreted results and prepared the manuscript. N. P. B. and J. A. R. conceptualized and supervised the research.

CONFLICTS OF INTEREST

There are no conflicts of interest to declare.

ACKNOWLEDGEMENTS

This work was primarily supported by the Assistant Secretary for Energy Efficiency and Renewable Energy, Vehicle Technologies Office, of the U.S. Department of Energy under Contract DE-AC02-05CH11231, under the Low Temperature Electrolyte program. D. M. H. and J. A. R. acknowledge the Joint Center for Energy Storage Research, an Energy Innovation Hub funded by the U.S. Department of Energy. A. S. H. was supported by a National Science Foundation Graduate Research Fellowship DGE-2020294884. Hard X-ray experiments were performed at the Advanced Light Source, which is supported by the Director, Office of Science, Office of Basic Energy Sciences, of the U.S. Department of Energy under Contract No. DE-AC02-05CH11231. Helen Bergstrom is also gratefully acknowledged for helpful discussions and suggestions.

BIBLIOGRAPHY

[1] Goodenough, J. B.; Kim, Y. Challenges for Rechargeable Li Batteries. *Chemistry of Materials* **2009**, *22* (3), 587–603.

[2] Newman, J. S.; Balsara, N. P. *Electrochemical Systems*; John Wiley & Sons Inc., 2021.

[3] Ma, Y.; Doyle, M.; Fuller, T. F.; Doeff, M. M.; De Jonghe, L. C.; Newman, J. The Measurement of a Complete Set of Transport Properties for a Concentrated Solid Polymer Electrolyte Solution. *Journal of The Electrochemical Society* **1995**, *142* (6), 1859–1868.

[4] Pesko, D. M.; Sawhney, S.; Newman, J.; Balsara, N. P. Comparing Two Electrochemical Approaches for Measuring Transference Numbers in Concentrated Electrolytes. *Journal of The Electrochemical Society* **2018**, *165* (13).

[5] Hou, T.; Monroe, C. W. Composition-Dependent Thermodynamic and Mass-Transport Characterization of Lithium Hexafluorophosphate in Propylene Carbonate. *Electrochimica Acta* **2020**, *332*, 135085.

[6] Landesfeind, J.; Gasteiger, H. A. Temperature and Concentration Dependence of the Ionic Transport Properties of Lithium-Ion Battery Electrolytes. *Journal of The Electrochemical Society* **2019**, *166* (14).

[7] Craig, N.; Mullin, S. A.; Pratt, R.; Crane, G. B. Determination of Transference Number and Thermodynamic Factor by Use of Anion-Exchange Concentration Cells and Concentration Cells. *Journal of The Electrochemical Society* **2019**, *166* (13).

[8] Stewart, S.; Newman, J. Measuring the Salt Activity Coefficient in Lithium-Battery Electrolytes. *Journal of The Electrochemical Society* **2008**, *155* (6).

[9] Bruce, P. G.; Vincent, C. A. Steady State Current Flow in Solid Binary Electrolyte Cells. *Journal of Electroanalytical Chemistry and Interfacial Electrochemistry* **1987**, *225* (1-2), 1–17.

[10] Evans, J.; Vincent, C. A.; Bruce, P. G. Electrochemical Measurement of Transference Numbers in Polymer Electrolytes. *Polymer* **1987**, *28* (13), 2324–2328.

[11] Watanabe, M.; Ogata, N.; Sanui, K.; Nagano, S. Estimation of Li+ Transport Number in Polymer Electrolytes by the Combination of Complex Impedance and Potentiostatic Polarization Measurements. *Solid State Ionics* **1988**, *28-30*, 911–917.

[12] Gao, K. W.; Balsara, N. P. Electrochemical Properties of Poly(Ethylene Oxide) Electrolytes above the Entanglement Threshold. *Solid State Ionics* **2021**, *364*, 115609.

[13] Frenck, L.; Sethi, G. K.; Maslyn, J. A.; Balsara, N. P. Factors That Control the Formation of Dendrites and Other Morphologies on Lithium Metal Anodes. *Frontiers in Energy Research* **2019**, *7*.

[14] Brissot, C.; Rosso, M.; Chazalviel, J.-N.; Baudry, P.; Lascaud, S. In Situ Study of Dendritic Growth in Lithium/PEO-Salt/Lithium Cells. *Electrochimica Acta* **1998**, *43* (10-11), 1569–1574.

[15] Ueno, K.; Yoshida, K.; Tsuchiya, M.; Tachikawa, N.; Dokko, K.; Watanabe, M. Glyme–Lithium Salt Equimolar Molten Mixtures: Concentrated Solutions or Solvate Ionic Liquids? *The Journal of Physical Chemistry B* **2012**, *116* (36), 11323–11331.

[16] Zhang, C.; Ueno, K.; Yamazaki, A.; Yoshida, K.; Moon, H.; Mandai, T.; Umebayashi, Y.; Dokko, K.; Watanabe, M. Chelate Effects in Glyme/Lithium Bis(Trifluoromethanesulfonyl)Amide Solvate Ionic Liquids. I. Stability of Solvate Cations and Correlation with Electrolyte Properties. *The Journal of Physical Chemistry B* **2014**, *118* (19), 5144–5153.

[17] Schmidt, F.; Schönhoff, M. Solvate Cation Migration and Ion Correlations in Solvate Ionic Liquids. *The Journal of Physical Chemistry B* **2020**, *124* (7), 1245–1252.

[18] Grundy, L. S.; Shah, D. B.; Nguyen, H. Q.; Diederichsen, K. M.; Celik, H.; DeSimone, J. M.; McCloskey, B. D.; Balsara, N. P. Impact of Frictional Interactions on Conductivity, Diffusion, and Transference Number in Ether- and Perfluoroether-Based Electrolytes. *Journal of The Electrochemical Society* **2020**, *167* (12), 120540.

[19] Holz, M. Electrophoretic NMR. *Chemical Society Reviews* **1994**, *23* (3), 165.

[20] Walls, H. J.; Zawodzinski, T. A. Anion and Cation Transference Numbers Determined by Electrophoretic NMR of Polymer Electrolytes Sum to Unity. *Electrochemical and Solid-State Letters* **1999**, *3* (7), 321.

[21] Gouverneur, M.; Kopp, J.; van Wüllen, L.; Schönhoff, M. Direct Determination of Ionic Transference Numbers in Ionic Liquids by Electrophoretic NMR. *Physical Chemistry Chemical Physics* **2015**, *17* (45), 30680–30686.

[22] Timachova, K.; Newman, J.; Balsara, N. P. Theoretical Interpretation of Ion Velocities in Concentrated Electrolytes Measured by Electrophoretic NMR. *Journal of The Electrochemical Society* **2019**, *166* (2).

[23] Pietsch, P.; Wood, V. X-Ray Tomography for Lithium Ion Battery Research: A Practical Guide. *Annual Review of Materials Research* **2017**, *47* (1), 451–479.

[24] Pietsch, P.; Westhoff, D.; Feinauer, J.; Eller, J.; Marone, F.; Stampanoni, M.; Schmidt, V.; Wood, V. Quantifying Microstructural Dynamics and Electrochemical Activity of Graphite and Silicon-Graphite Lithium Ion Battery Anodes. *Nature Communications* **2016**, *7* (1).

[25] Sun, F.; Zielke, L.; Markötter, H.; Hilger, A.; Zhou, D.; Moroni, R.; Zengerle, R.; Thiele, S.; Banhart, J.; Manke, I. Morphological Evolution of Electrochemically Plated/Stripped Lithium Microstructures Investigated by Synchrotron X-Ray Phase Contrast Tomography. *ACS Nano* **2016**, *10* (8), 7990–7997.

[26] Sun, F.; Moroni, R.; Dong, K.; Markötter, H.; Zhou, D.; Hilger, A.; Zielke, L.; Zengerle, R.; Thiele, S.; Banhart, J.; Manke, I. Study of the Mechanisms of Internal Short Circuit in a Li/Li Cell by Synchrotron X-Ray Phase Contrast Tomography. *ACS Energy Letters* **2016**, *2* (1), 94–104.

[27] Harry, K. J.; Hallinan, D. T.; Parkinson, D. Y.; MacDowell, A. A.; Balsara, N. P. Detection of Subsurface Structures underneath Dendrites Formed on Cycled Lithium Metal Electrodes. *Nature Materials* **2013**, *13* (1), 69–73.

[28] Shah, D. B.; Nguyen, H. Q.; Grundy, L. S.; Olson, K. R.; Mecham, S. J.; DeSimone, J. M.; Balsara, N. P. Difference between Approximate and Rigorously Measured Transference Numbers in Fluorinated Electrolytes. *Physical Chemistry Chemical Physics* **2019**, *21* (15), 7857–7866.

[29] Galluzzo, M. D.; Maslyn, J. A.; Shah, D. B.; Balsara, N. P. Ohm's Law for Ion Conduction in Lithium and Beyond-Lithium Battery Electrolytes. *The Journal of Chemical Physics.* **2019**, *151* (2), 020901.

[30] Newman, J.; Chapman, T. W. Restricted Diffusion in Binary Solutions. *AIChE Journal* **1973**, *19* (2), 343–348.

[31] Thompson, S. D.; Newman, J. Differential Diffusion Coefficients of Sodium Polysulfide Melts. *Journal of The Electrochemical Society* **1989**, *136* (11), 3362–3369.

[32] Ho, A. S.; Parkinson, D. Y.; Finegan, D. P.; Trask, S. E.; Jansen, A. N.; Tong, W.; Balsara, N. P. 3D Detection of Lithiation and Lithium Plating in Graphite Anodes during Fast Charging. *ACS Nano* **2021**, *15* (6), 10480–10487.

[33] Maslyn, J. A.; Frenck, L.; Veeraraghavan, V. D.; Müller, A.; Ho, A. S.; Marwaha, N.; Loo, W. S.; Parkinson, D. Y.; Minor, A. M.; Balsara, N. P. Limiting Current in Nanostructured Block Copolymer Electrolytes. *Macromolecules* **2021**, *54*(9), 4010–4022.

[34] Halat, D. M.; Fang, C.; Hickson, D.; Mistry, A.; Reimer, J. A.; Balsara, N. P.; Wang, R. Electric-Field-Induced Spatially Dynamic Heterogeneity of Solvent Motion and Cation Transference in Electrolytes. *Physical Review Letters* **2022**, *128* (19).

[35] Hallberg, F.; Furó, I.; Yushmanov, P. V.; Stilbs, P. Sensitive and Robust Electrophoretic NMR: Instrumentation and Experiments. *Journal of Magnetic Resonance* **2008**, *192* (1), 69–77.

[36] Fawdon, J.; Ihli, J.; Mantia, F. L.; Pasta, M. Characterising Lithium-Ion Electrolytes via Operando Raman Microspectroscopy. *Nature Communications* **2021**, *12* (1).

[37] Stewart, S. G.; Newman, J. The Use of UV/Vis Absorption to Measure Diffusion Coefficients in $LiPF_6$ Electrolytic Solutions. *Journal of The Electrochemical Society* **2008**, *155* (1).

[38] Valøen Lars Ole; Reimers, J. N. Transport Properties of $LiPF_6$-Based Li-Ion Battery Electrolytes. *Journal of The Electrochemical Society* **2005**, *152* (5).

[39] Balsara, N. P.; Newman, J. Relationship between Steady-State Current in Symmetric Cells and Transference Number of Electrolytes Comprising Univalent and Multivalent Ions. *Journal of The Electrochemical Society* **2015**, *162* (14).

[40] Pesko, D. M.; Timachova, K.; Bhattacharya, R.; Smith, M. C.; Villaluenga, I.; Newman, J.; Balsara, N. P. Negative Transference Numbers in Poly(Ethylene Oxide)-Based Electrolytes. *Journal of The Electrochemical Society* **2017**, *164* (11).

[41] Michael Galluzzo, *Salt Concentration Gradients in Block Copolymer Electrolytes. UC Berkeley*, Thesis, University of California, Berkeley, 2021. Retrieved from https://escholarship.org/uc/item/67c3087r

[42] Loo, W. S.; Fang, C.; Balsara, N. P.; Wang, R. Uncovering Local Correlations in Polymer Electrolytes by X-Ray Scattering and Molecular Dynamics Simulations. *Macromolecules* **2021**, *54* (14), 6639–6648.

[43] France-Lanord, A.; Grossman, J. C. Correlations from Ion Pairing and the Nernst-Einstein Equation. *Physical Review Letters* **2019**, *122* (13).

[44] Nilsson, V.; Bernin, D.; Brandell, D.; Edström, K.; Johansson, P. Interactions and Transport in Highly Concentrated LiTFSI-Based Electrolytes. *ChemPhysChem* **2020**, *21* (11), 1166–1176.

[45] Debye, P.; Hückel, E. Zur Theorie der Elektrolyte. *Physikalische Zeitschrift* **1923**, *24* (9), 185-206.

Symbol List

κ	Ionic conductivity (S cm^{-1})
D	Salt diffusion coefficient (cm^2 s^{-1})
$t_{+¿^0¿}$	Cation transference number with respect to the solvent velocity
T_f	Thermodynamic factor
$\gamma_{\pm ¿¿}$	Mean molar activity coefficient
m	Molality (mol kg^{-1})
U	Open circuit potential (mV)
F	Faraday's constant (C mol^{-1})
m_r	Reference molality (mol kg^{-1})
R	Universal gas constant (8.314 J mol^{-1} K^{-1})
T	Temperature (°C)
$t_{-¿^0¿}$	Anion transference number
i	Current density (mA cm^{-2})

t	Time (s)
U_{ci}	Open circuit potential from current interrupt technique (mV)
$\rho_{+¿¿}$	Current fraction
$v_{+¿¿}$	Cation velocity (μm cm^{-1})
$v_{-¿¿}$	Anion velocity (μm cm^{-1})
v_0	Solvent velocity (μm cm^{-1})
r	Measure of ratio of lithium ions to oxygen atoms in solvent
τ	Tortuosity of separator
φ_c	Volume fraction of conducting phase in separator
l	Thickness of the separator (cm)
R_s	Series resistance (Ω)
A	Area of electrodes (cm^2)
ΔV	Applied polarization potential (mV)
I_{ss}	Steady state current (mA)
I_Ω	Initial current calculated via Ohm's law, $I_\Omega = \Delta V / R_T$ (mA)
$R_{i,0}$	Initial interfacial resistance (Ω)
$R_{i,ss}$	Steady state interfacial resistance (Ω)
k_0	Offset voltage (mV)
a	Fit parameter for restricted diffusion
b	Fit parameter for restricted diffusion